HORIZON EUROPE PROGRAMME
HORIZON-CL5-2023-D3-02-11

GA No. 101147275

Silicon solar cells with Low Environmental footprint and Advanced interfaces

SiLEAN - Deliverable report

D4.2 – > 25% solar cell with ZnO as TCO

Funded by
the European Union

Deliverable No.	D4.2	
Related WP	WP4	
Deliverable Title	> 25% solar cell with ZnO as TCO	
Deliverable Date	2026-04-30	
Deliverable Type	REPORT	
Dissemination level	Public (PU)	
Author(s)	Alexandr Zamchiy (FZJ), Gökhan Altıner (GUNAM)	2025-04-9
Checked by	Valerie Depauw (IMEC)	2026-04-23
Reviewed by	Olindo Isabella (TUD)	2026-04-28
Approved by	Karsten Bittkau (FZJ) - Project Coordinator	2026-04-30
Status	Final	2026-04-30

Document History

Version	Date	Editing done by	Remarks
V1.0	27/04/26	Alexandr Zamchiy (FZJ), Gökhan Altıner (GÜNAM), Valérie Depauw (IMEC)	First version
V1.1	29/04/26	Alexandr Zamchiy (FZJ), Gökhan Altıner (GÜNAM)	Revision
V2.0	30/04/26	Valérie Depauw (IMEC), Karsten Bittkau (FZJ)	Second version
FINAL	30/04/26	Dion Terwiel, Anna Molinari (UNR)	Clean

Project Scientific Abstract

The SiLEAN project deals with the development of advanced innovations to tackle the major drawbacks of silicon heterojunction solar cell technology, namely the high energy and material demand for Si wafer manufacturing, limited current generation, and the consumption of scarce materials like silver, bismuth and indium. Within the scope of the project, we will directly grow the wafers from the gas phase with low temperature processes, apply alternative passivation concepts that show higher optical transparency, develop indium-free contact layers and apply silver and bismuth-free metallization with all-in-one cell interconnection and encapsulation. The project aims to achieve >25.5% solar cell efficiency and >23.5% module efficiency with 50% lower costs for Si wafers and contacting, as well as up to 75% lower carbon footprint. All processes applied allow upscaling to larger sizes as well as high manufacturing throughput. Eventually, the developments of SiLEAN will pave the way for a new, lean, generation of heterojunction solar cell technology that will both increment the energy conversion efficiency and unlock production at terawatt-scale.

Public summary

One of the key objectives of the SiLEAN project is the replacement of the state-of-the-art indium (In)-based contact layers with more cost-effective indium-free alternatives in silicon heterojunction (SHJ) solar cells. The investigated approaches include indium-free transparent conductive oxides (TCOs) based on undoped zinc oxide (ZnO) deposited by plasma-enhanced chemical vapor deposition (PECVD), aluminium-doped ZnO (AZO) deposited by spatial atomic layer deposition (sALD), and, subsequently, tin oxide (SnO_X) deposited by magnetron sputtering.

This deliverable, prepared 24 months after the project start, summarizes the progress towards achieving SHJ solar cells efficiencies above 25% using indium-free TCOs and analyses the key challenges associated with their implementation.

Optimization of the PECVD process enabled the development of a baseline recipe for undoped ZnO, which was successfully integrated as a contact layer in SHJ devices in combination with sputtered AZO and indium-doped tin oxide (ITO) seed and capping layers. However, due to a significant decrease in the undoped PECVD ZnO deposition rate, it was decided to shift toward the development of an alternative indium-free contact layer, SnO_X, deposited by sputtering.

The optoelectronic properties of SnO_X films were optimized, and the layers were implemented in SHJ solar cells, yielding a champion power conversion efficiency (PCE) of 22.0% for fully indium-free devices. It was found that the main limitation of SnO_X-based SHJ devices is the relatively high contact resistivity at SnO_X/amorphous silicon interface, which reduces the fill factor. This limitation was effectively mitigated by introducing a thin (10 nm) ITO seed layer, resulting in a champion PCE of 23.4%. This efficiency is comparable within the error margin to 23.3% for reference ITO-based SHJ solar cells, but is achieved with 80% less In content.

Further improvements in PCE are expected through the replacement of doped amorphous silicon with nanocrystalline silicon (oxide) layers, the incorporation of indium-free interlayers with improved contact properties (e.g., sputtered and/or sALD-grown AZO), optimization of heat-assisted light soaking process, and upscaling of SnO_X sputtering to industrially relevant M2/$M2^+$ wafer sizes.

Contents

List of Figures

List of Tables

Abbreviations & Definitions

Abbreviation	Explanation
sALD	Spatial atomic layer deposition
a-Si:H	Hydrogenated amorphous silicon
AZO	Aluminium-doped zinc oxide
CO_2	Carbon dioxide
Cz wafer	Czochralski wafer
DEZ	Diethylzinc
DMAI	Dimethylaluminum isopropoxide
FF	Fill factor
GAZO	Gallium and aluminium co-doped zinc oxide
ITO	Indium-doped tin oxide
J_{loss}	Current loss density
LiSo	Heat-assisted Light Soaking
nc-Si(O_X):H	Nanocrystalline silicon (oxide)
PCE	Power conversion efficiency
PECVD	Plasma-enhanced chemical vapor deposition
r	Oxygen flow ratio
RF	Radiofrequency
R_S	Series resistance
SHJ	Silicon heterojunction
SnO_X	Tin oxide
TCO	Transparent conductive oxide
TLM	Transfer length method
V_{OC}	Open-circuit voltage

1 Introduction

SiLEAN partners are developing indium-free transparent conductive oxides (TCOs) which are used in silicon heterojunction (SHJ) solar cells as transparent electrodes (Figure 1). Within the framework of the SiLEAN project, alternative concepts to state-of-the-art indium-based TCOs (such as indium-doped tin oxide (ITO)) have been explored. These includes indium-free approaches based on undoped zinc oxide (ZnO) deposited by plasma-enhanced chemical vapor deposition (PECVD), aluminium-doped ZnO (AZO) deposited by spatial atomic layer deposition (sALD), and, subsequently, tin oxide (SnO_X) deposited by magnetron sputtering as an alternative indium-free contact layer to PECVD ZnO.

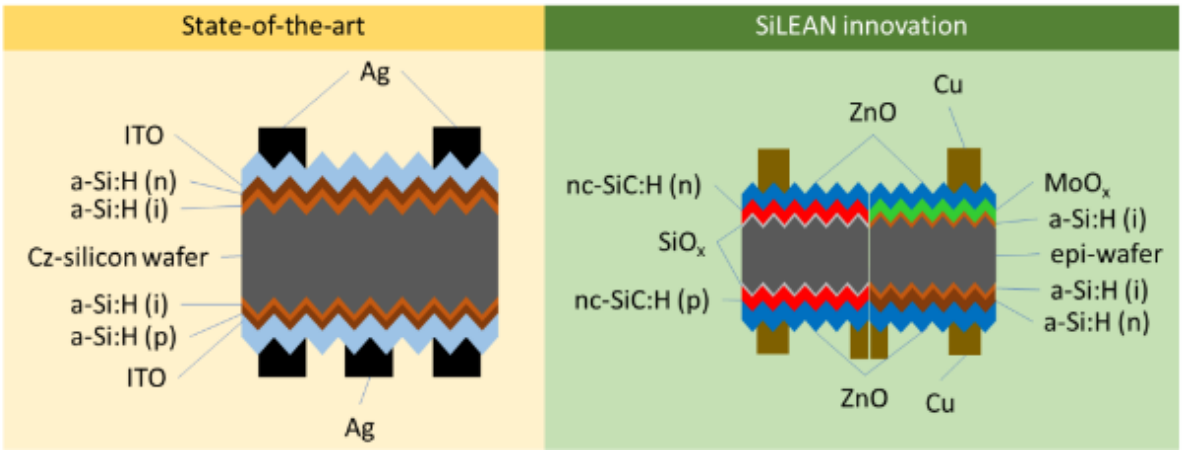

Figure 1: State-of-the-art (left) and SiLEAN innovation (right) at SHJ solar-cell level.

The deliverable is part of Work Package 4 which focuses on developing contacting schemes that minimize reliance on critical raw materials. It has been realized through close collaboration between FZJ, GUNAM, and 3SUN. The role of FZJ was to optimize the optoelectronic properties of undoped PECVD ZnO and sputtered SnO_X films, as well as to implement them in SHJ solar cells as contact layers in indium-free and indium-lean configurations. The role of 3SUN was to provide a-Si:H(n)/a-Si:H(i)/c-Si(n)/a-Si:H(i)/a-Si:H(p) stacks for testing the contact layers in various configurations at the device level at FZJ. Prepared 24 months after the start of the project, the **purpose of this deliverable**, is to summarize the progress towards achieving SHJ solar cells efficiencies above 25% using indium-free TCOs, and to provide an analysis of the challenges encountered in the development and implementation of these materials on the path towards the defined target performance.

In the initial phase of the study, optimization of the PECVD process resulted in the development of a baseline recipe for undoped ZnO (Section 2.2). Further, the PECVD films were applied as contact layers in SHJ solar cells in combination with sputtered AZO and ITO, which were used as seed and capping layers, respectively. Later, due to the emergence of a significant technical issue related to PECVD ZnO – namely, a decrease in the deposition rate – it was decided to shift toward the development of an alternative indium-free contact layer, SnO_X, deposited by sputtering (Section 2.3). The optoelectronic properties of SnO_X films were optimized, and the optimized films were subsequently employed as contact layers in SHJ solar cells.

Additionally, sALD-grown indium-free AZO layers were developed at GUNAM to serve as alternative TCOs in SHJ structures (Section 2.4). The sALD process provides atomic-level thickness control and generally offers superior uniformity and conformality with respect to conventional PECVD and sputtering techniques. The optoelectronic properties of the stand-alone AZO layers have been characterized; however, at the time of writing this deliverable report, the AZO layers have not yet been implemented on SHJ cells. Consequently, device-level integration and testing will be conducted in the subsequent project phase (cf. **D4.6**).

2 Results & Discussion

2.1 Experimental details

Undoped ZnO films were deposited via PECVD. Diethylzinc (DEZ, $(C_2H_5)_2Zn$) and carbon dioxide (CO_2) were used as zinc and oxygen precursors, respectively. DEZ was introduced into the deposition chamber via a bubbler system using argon as the carrier gas.

SnO_X films were sputtered at different RF power conditions (75, 100, 150, and 200 W), corresponding to power densities of 0.59, 0.79, 1.18, and 1.58 W/cm^2, respectively, as a function of the oxygen flow ratio r = O_2 flow rate / (O_2 flow rate + Ar flow rate) at room temperature. The thicknesses of the undoped PECVD ZnO and sputtered SnO_X on glass for optoelectrical characterization were ≈ 100 nm. The thickness of AZO, gallium and aluminum co-doped zinc oxide (GAZO), and ITO prepared by magnetron sputtering and used as seed and capping layers was ≈ 10 - 15 nm.

sALD AZO films were prepared using a sALD tool by SALD BV. DEZ and dimethylaluminum isopropoxide (DMAI) were employed as precursors for ZnO deposition and Al doping, respectively, with H_2O serving as the co-reactant. The AZO layers were prepared by the co-injection method, where both precursors are deposited simultaneously. The deposition was realized at 230 °C, with a fixed DEZ flow of 0.5 slm and varying DMAI flows to obtain different Al doping ratios. Different DMAI flows were achieved by keeping the DMAI flow from the precursor vessel fixed at 0.2 slm while varying the N_2 dilution flow to 2.5, 9, and 18 slm in order to get low, medium, and high Al doping concentrations, respectively. The dilution flow was increased rather than reducing the precursor flow directly, as DMAI flows below 0.2 slm were observed to cause mechanical instability in the tool. Optical transmittance was measured using a photovoltaic characterization system (PV300, Bentham Instruments), and sheet resistance was measured on glass substrates coated with > 80 nm AZO using a four-point probe (FPP-Scan, PV-Tools). Thickness and optical constants (n-k) were determined via variable-angle spectroscopic ellipsometry (VASE – GES5E, Semilab) using the Tauc-Lorentz dispersion law with a Drude oscillation model [1].

To fabricate **SHJ solar cells** (2x2 cm^2), double-textured Cz-grown n-type <100> c-Si wafers supplied by LONGi with a crystallographic orientation of <100>, a resistivity of 1 Ω·cm, and a thickness of 135 µm were used. Intrinsic (a-Si:H(i)) and doped (a-Si:H(p) and a-Si:H(n)) amorphous silicon films were prepared by PECVD at FZJ. Moreover, for the fabrication of SHJ solar cells with SnO_X and ITO/SnO_X contact layers, a-Si:H(n)/a-Si:H(i)/c-Si(n)/a-Si:H(i)/a-Si:H(p) stacks provided by 3SUN were used on double-textured Cz-grown n-type <100> c-Si wafers with a resistivity of 0.55 Ω·cm, and a thickness of 155 µm.

2.2 Undoped ZnO fabricated by PECVD

At the initial stage of the study, optimization of the PECVD process led to the establishment of a baseline recipe for undoped ZnO. Introducing boron as a dopant added further complexity to the newly developed process; therefore, the initial focus was placed on investigating undoped ZnO films. The layers exhibited optical transparency similar to that of sputtered ZnO films. However, the films showed low electron mobility (< 6 m^2/V·s) resulting in relatively high resistivity (≈ 2*10^{-2} Ω cm, vs. ≈ 4*10^{-4} Ω cm for ITO). Furthermore, air annealing at 170 °C for 40 min was found to significantly deteriorate further the electrical performance of the films (Figure 2a-c). It was demonstrated that introducing a thin seed layer (≈ 15 nm), e.g. ITO, AZO, GAZO, can substantially improve the electrical

properties – particularly carrier mobility - and reduce the degradation of electrical performance during annealing.

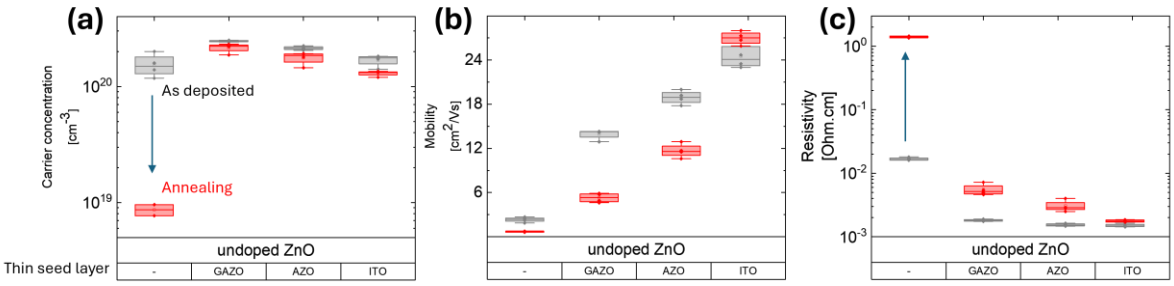

Figure 2: Opto-electrical properties of undoped ZnO fabricated by PECVD with and without seed layers: (a) charge carrier concentration, (b) charge carrier mobility, (c) resistivity.

The undoped PECVD ZnO films were subsequently integrated into SHJ solar cells, with device performance summarized in Figure 3 and Table 1. Various TCO stacking configurations were implemented on the front side of the SHJ structure (Figure 3), while ITO was employed on the rear side of the devices. Overall, the efficiency of the solar cells incorporating undoped PECVD ZnO contact layer (structure 1) was limited by a low fill factor (FF), primarily caused by high series resistance (R_S) (Table 1). This issue, and especially the S-shape related to a barrier layer between ZnO and i/n a-Si:H, was alleviated by introducing a seed layer. Devices with a sputtered AZO seed layer (structure 2) exhibited a significant improvement in FF. The addition of a capping layer of ITO (structure 3) further enhanced the FF and reduced the R_S. However, the open-circuit voltage (V_{oc}) remained below 700 mV, representing an additional limitation. Further investigation is required to understand the impact of undoped PECVD ZnO on the passivation layers in SHJ solar cell precursors and to develop strategies to mitigate this effect.

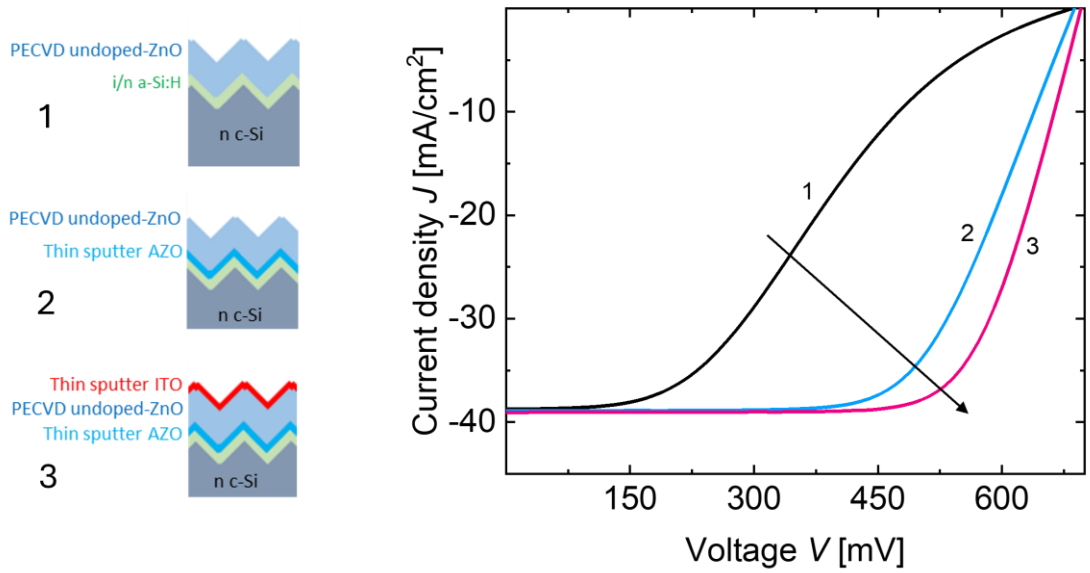

Figure 3: Side-view schematic of the front-side structure of SHJ solar cells with different TCO configurations, along with the corresponding J-V curves of devices employing these configurations.

At the GA meeting in May 2025 (M13), a significant technical issue associated with PECVD ZnO was reported, namely a pronounced reduction in the deposition rate of the films. The current process requires approximately 8 hours to deposit a ~70 nm ZnO film on a textured wafer (previously, the typical deposition time was approximately 1 hour), rendering it impractical for systematic studies aimed at process optimization or for application in SHJ solar cels. To identify the root cause and

implement corrective measures, it was decided to open the deposition chamber. However, this procedure necessitates special attention due to the toxicity and pyrophoricity of the DEZ precursor. As for today, no fully validated safety protocol has yet been established. Consequently, the timeline for resuming PECVD ZnO research remains uncertain.

Table 1: Electrical performance parameters of SHJ solar cells employing undoped PECVD ZnO.

Structure	V_{OC} [mV]	J_{SC} [mA/cm^2]	FF [%]	R_S [Ohm.cm^2]	PCE [%]
1 | Undoped ZnO	685	38.7	32.7	6.1	8.7
2 | AZO-seeded undoped ZnO	688	38.9	64.2	3.2	17.2
3 | ITO-seeded undoped ZnO	696	39.0	71.3	2.0	19.4
4 | Reference ITO	731	39.1	79.1	0.5	22.6

In summary, a new approach for depositing indium-free TCO layers via PECVD of undoped ZnO thin films was established, and their opto-electrical properties were systematically characterized. The as-deposited undoped ZnO films exhibited high resistivity and poor stability under air annealing. Introducing GAZO, AZO, and ITO seed layers was shown to effectively address this issue. The integration of the PECVD process into SHJ solar cell fabrication was successfully demonstrated, highlighting the benefits of seed layers in improving device performance. Devices with a single-layer front-side undoped PECVD contact exhibited a power conversion efficiency (PCE) of 8.7%. Then, introducing AZO and ITO as seed and capping layers, respectively, enabled an increase in PCE to 19.4%. Thus, further optimization of the PECVD conditions is required to maximize cell efficiency, which is decided not to do due to the technical issue mentioned above.

2.3 Sputtered SnO_X

As an alternative indium-free contact layer to undoped PECVD ZnO, FZJ proposed the development of tin oxide (SnO_X) deposited by sputtering. It should be noted that PECVD-grown ZnO offers higher tunability compared to sputtered films, allowing more flexible adjustments of material properties during deposition [2, 3]. This capability can be leveraged to design advanced contact layers, such as composition- or/and structure-graded films and bilayer stacks. In addition, PECVD processing may help to avoid passivation damage commonly associated with sputtering. Replacing PECVD ZnO with sputtered SnO_X would therefore result in the loss of these advantages. However, it would simultaneously allow for higher throughput and improved stability under hot and humid conditions - limitations inherent to PECVD ZnO [4-6]. The issue of sputter damage in SnO_X is not considered prohibitive, particularly with use of RF sputtering regimes. Furthermore, preliminary studies indicate that sputtered SnO_X exhibits lower optical absorption in the 300 - 1300-nm wavelength range compared to reference sputtered AZO and ITO films. At the same time, its electrical properties (mobility > 15 cm^2/Vs and carrier density > 1.5*10^{20} cm^{-3}) are already well suited for application in solar cells.

2.3.1 Optimisation of the SnO_X deposition conditions

At the initial stage, the properties of the layers were systematically investigated as a function of key sputtering parameters (power, pressure, substrate temperature, and gas mixture composition). Figure 4 presents the optoelectrical properties of SnO_X films (~95 -105 nm) deposited at different RF powers (75, 100, 150, and 200 W), corresponding to power densities of 0.59, 0.79, 1.18, and 1.58 W/cm^2, respectively, plotted as a function of the oxygen flow ratio r = O_2 flow rate / (O_2 flow rate + Ar flow rate) at room temperature, both before and after annealing at 180 - 200 °C.

For the films deposited at various power levels, an increase in oxygen leads to a reduction in resistivity (Figure 4a), reaching a minimum of ~2.5*10^{-3} Ω cm. Notably, this minimum occurs at different r values for different applied power. Concurrently, the carrier density and mobility increase, attaining maximum values of approximately 1.8*10^{20} cm^{-3} and 17 cm^2/Vs, respectively. For each power condition, these maxima are observed at distinct oxygen flow ratios. A further increase in r results in a decline in both carrier density and mobility, leading to an increase in resistivity. The behaviour can be attributed to the formation of oxygen vacancies and undercoordinated Sn atoms (acting as a shallow donor states) under moderately oxygen-deficient conditions, which enhance conductivity. In contrast, excess oxygen promotes the formation of interstitial oxygen or O-O species, which act as trap states and introduce structural disorder, thereby degrading the electrical conductivity.

For films deposited under varying sputtering power and oxygen flow ratio conditions on glass substrates, the spectral dependence of the absorption coefficient in the 300 – 1300 nm range was used to estimate current loss densities (J_{loss}):

$$J_{loss} = \int_{1300}^{300} \left(1 - e^{-\alpha(\lambda)\cdot d}\right) AM1.5G(\lambda)\, d\lambda$$

where $\alpha(\lambda)$ and $AM1.5G(\lambda)$ denote the absorption coefficient of SnO_X and the global standard terrestrial solar spectrum, respectively, as functions of wavelength. A layer thickness (d) of 70 nm is assumed. Figure 4b shows the relationship between sheet resistance and J_{loss}. It can be observed that, at certain oxygen flow ratios, the parasitic absorption losses in SnO_X are lower than those of reference ITO, while simultaneously exhibiting superior optoelectrical performance compared to reference sputtered AZO.

Furthermore, post-annealing in an oxygen-free atmosphere was shown to effectively mitigate degradation induced by energetic O^- ion bombardment. This treatment enhances the electrical properties and enables the use of more optically thin films in solar cells. For example, at a deposition power density of 0.79 W/cm^2, the resistivity after annealing at 180 – 200 °C reached 1.6*10^{-3} Ω cm (vs. ~4*10^{-4} Ω cm for ITO) over a broad range of oxygen flow ratios (r = 0.6 – 1).

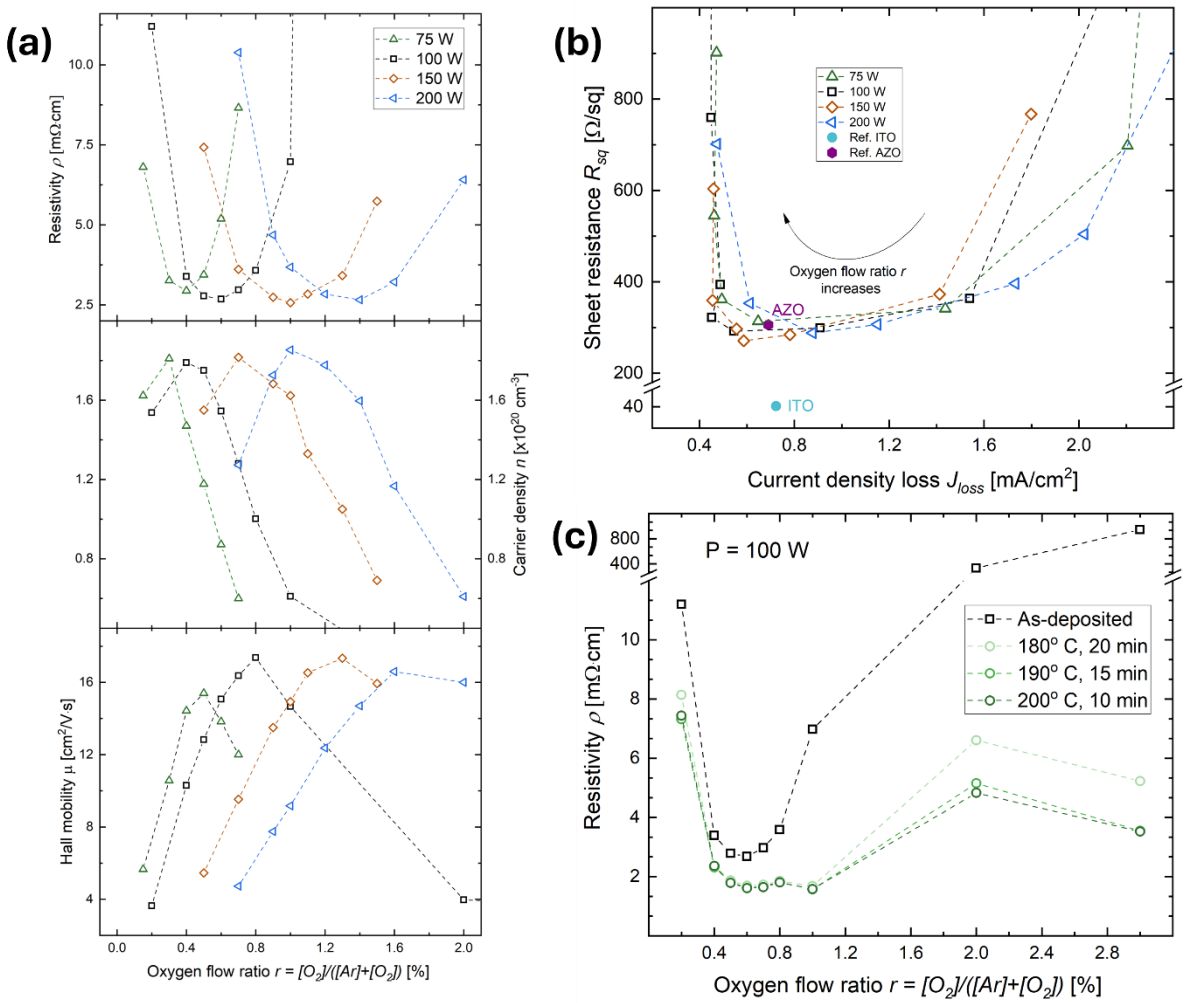

Figure 4: Optoelectrical properties of sputtered SnO_X:*(a) resistivity, carrier density, and hall mobility of the films varied with oxygen flow ratio before annealing, (b) sheet resistance versus current loss density, (c) resistivity of the films deposited at 100 W, as a function of oxygen flow ratio for as-deposited and annealed conditions.*

2.3.2 Solar cells with sputtered SnO_X as TCO

Two solar cell runs for SnO_X integration as TCO were performed. In the first run, SnO_X films deposited under optimized sputtering conditions (r = 0.4%, 75 W; r = 0.6%, 100 W; r = 1%, 150 W; r = 1.4%, 200 W) were employed as contact layers in indium-free SHJ solar cells. Figure 5 shows the parameters extracted from J-V measurements of 2x2 cm^2 SHJ solar cells with different TCO configurations, both before and after heat-assisted light soaking (LiSo) performed at 190 °C for 3 minutes. A significant increase in the average open-circuit voltage (V_{OC}) from 716 mV to 724 mV is observed before LiSo (Figure 5a) when the reference ITO, sputtered at 1000 W, is replaced by SnO_X sputtered at 75 W and 100 W. However, with a further increase in sputtering power to 150 W and 200 W, the average V_{OC} before LiSo decreases substantially to 710 mV and 680 mV, respectively, which can be attributed to increased sputter-induced damage. LiSo results in a pronounced improvement in V_{OC} for both reference ITO SHJ solar cells and the SnO_X-based devices. Notably, the V_{OC} values of the solar cells with SnO_X sputtered at 75 W - 732 mV and 100 W - 732mV, remain higher than the reference value - 728mV.

Indium-free SHJ solar cells with SnO_X sputtered at 75 W and 100 W exhibit higher average J_{SC} of 38.9 mA/cm^2 and 38.6 mA/cm^2, respectively, compared to the reference value of 38.4 mA/cm^2. This improvement is likely associated with reduced parasitic absorption in SnO_X relative to ITO (Figure 4b). However, with increasing sputtering power to 150 W and 200 W, J_{SC} decreases, which can be attributed to degraded charge-carrier collection, as evidenced by external quantum efficiency measurements (not shown here), and is related to severe sputter-induced damage under these

conditions. It is also noteworthy that a deterioration of J_{SC} is observed after LiSo, which appears to be characteristic of SnO_X-based SHJ solar cells. FF of SnO_X-based SHJ solar cells shows significantly lower average values (75.5% for 75 W and 76.3% for 100 W) compared to the reference devices (78.9%) prior to LiSo. With increasing sputter power to 150 W and 200 W, the average FF further decreases to 75.2% and 71.8%, respectively. The R_S of SnO_X-based SHJ solar cell is substantially higher than that of the reference devices, in full agreement with the trend observed for FF as a function of sputtering power (Figure 5b). Additionally, an increase in R_S is observed for indium-free solar cells after LiSo, which is not typical for ITO-based devices. Furthermore, it was observed (not shown here) that the stack of doped a-Si:H and SnO_X exhibits relatively high specific contact resistivity, which is likely the main factor limiting FF. Notably, the specific contact resistivity also increases after LiSo for SnO_X-based SHJ solar cells.

As a result, the average power conversion efficiency (PCE) for the mildest SnO_X sputtering conditions (75W and 100W) reached 21.2% and 21.3%, respectively, prior LiSo, and 21.3% and 21.5%, respectively, after LiSo. In comparison, the PCE values for the ITO-based reference devices were 21.8% and 22.4%, respectively.

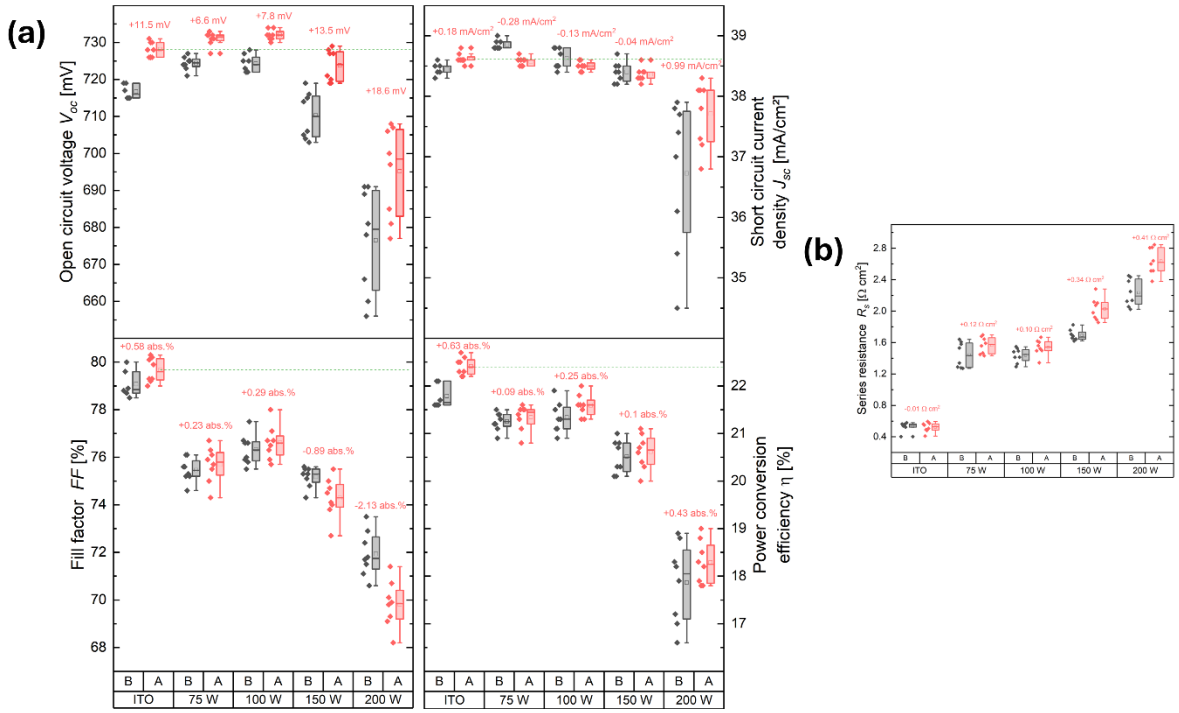

Figure 5: (a) Open-circuit voltage (V_{OC}), short-circuit current density (J_{SC}), fill factor (FF) ,and power conversion efficiency (PCE), and (b) series resistance (R_S) of 2x2 cm² solar cells with different TCO configurations, incorporating SnO_X sputtered at different power and ITO measured before (B, grey) and after (A, red) heat-assisted light soaking. The values shown in red illustrate the difference between the corresponding quantities after and before LiSo.

Next, SnO_X sputtering conditions identified earlier as the most optimal for application in SHJ solar cells (r = 0.6%, 100 W) were employed for the fabrication of 2x2 cm² devices based on a-Si:H(n)/a-Si:H(i)/c-Si(n)/a-Si:H(i)/a-Si:H(p) stacks provided by 3SUN, which exhibit a higher potential for achieving improved PCE, including ITO, SnO_X, and a bilayer structure of ITO (10 nm)/SnO_X.

Figure 6a-b present the parameters extracted from J-V measurements of SHJ solar cells with different TCO configurations. The higher V_{OC} of SnO_X-based solar cells compared to ITO-based ones is preserved. Introducing a 10-nm-thick ITO seed layer reduces V_{OC} relative to SnO_X after sputtering, however, after LiSo, V_{OC} values become nearly identical. J_{SC} values are similar across all configurations after LiSo.

The ITO seed layer significantly improves FF. For ITO/SnO_X devices, LiSo increases the average FF by 1.3 abs.% to 82.1%, while reference ITO-based solar cells show a compatible gain of 1.16 abs.% and an average FF value of 81.8%. In contrast, SnO_X-based devices exhibit negligible FF improvement (+0.14 abs.%), remaining significantly lower at 74.0%. The reduced FF is associated with higher R_S

(Figure 6b), which further increases after LiSo of SnO_X-based solar cells, unlike ITO-containing devices. Transfer length method (TLM) measurements of the specific contact resistivity values of the electron contact indicate that the Ag/TCO contact resistance is higher for SnO_X than for ITO (Figure 6c). For the full front stack, the average specific contact resistivity in the case of SnO_X (590 mΩcm^2) is significantly higher than that of ITO (225 mΩcm^2). The introduction of the ITO seed layer substantially reduces this value to the level of the reference (220 mΩcm^2), which is consistent with the trends in R_S and FF.

Overall, the incorporation of an ITO seed layer yields an average PCE of 23.06%, which is comparable to that of reference ITO-based SHJ solar cells (23.10%) after LiSo, while SnO_X-based devices achieve only 20.93%.

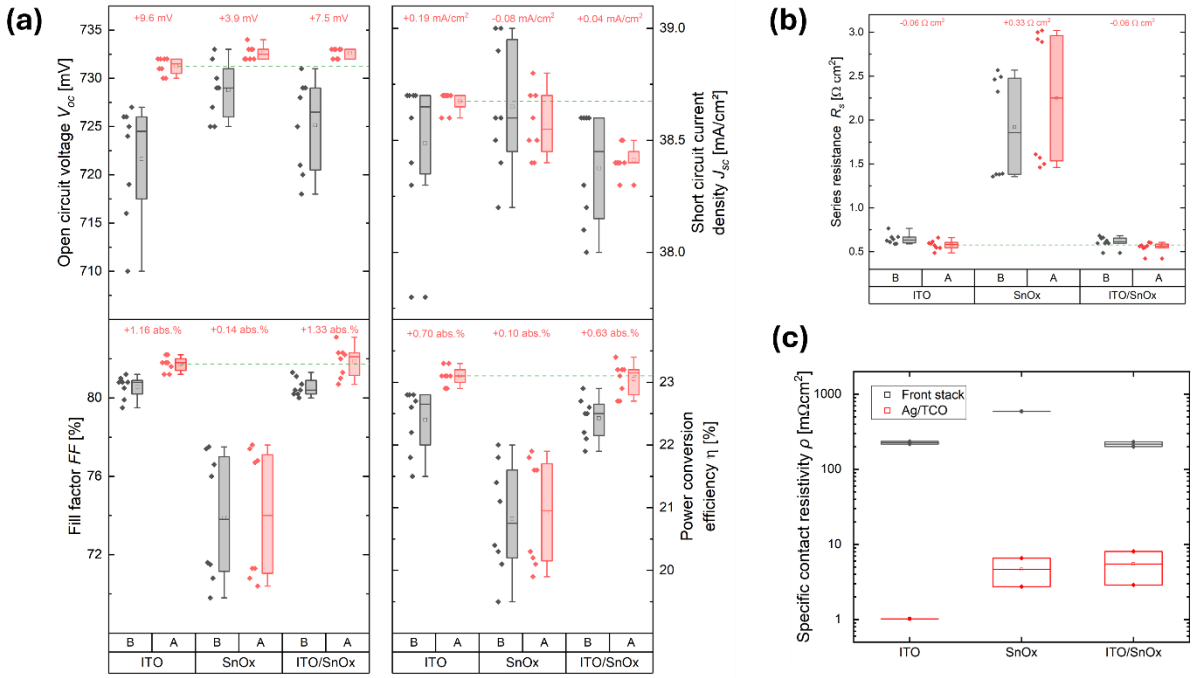

Figure 6: (a) Open-circuit voltage (V_{OC}), short-circuit current density (J_{SC}), fill factor (FF), and power conversion efficiency (PCE), (b) series resistance (R_S) of 2x2 cm^2 solar cells fabricated using a-Si:H(n)/a-Si:H(i)/c-Si(n)/a-Si:H(i)/a-Si:H(p) stacks provided by 3SUN, with different TCO configurations, measured before (B, grey) and after (A, red) LiSo, and (c) specific contact resistivities of electron. contact for different TCO configurations after LiSo. The values shown in red illustrate the difference between the corresponding quantities after and before LiSo.

In summary, it is shown that the main obstacle to achieving PCE values comparable to those of reference ITO-based SHJ solar cells when using SnO_X as a contact layer is the relatively high contact resistivity of the SnO_X/a-Si:H contact, which limits the device FF due to a larger Schottky barrier at the interface. It is further demonstrated that this issue can be significantly mitigated by introducing a thin (10 nm) ITO layer. For 2x2 cm^2 devices, champion efficiencies of 22.0% and 23.4% were achieved for SnO_X- and ITO/SnO_X-based SHJ solar cells, respectively, compared with 23.3% for reference ITO-based devices, which is still far from the target of > 25.0% defined in the deliverable. To further decrease the contact resistivity and thus increase the PCE, SnO_X-based devices within the indium-free SHJ solar cell concept, replacement of doped a-Si:H with nanocrystalline silicon (oxide) (nc-Si(O_x):H) layers as well as the introduction of indium-free seed layers (e.g., AZO) will be implemented. These approaches are well aligned with other ongoing project activities, such as the development of a transparent passivating front contact based on nc-SiO_x:H at FZJ within Work Package 3, and sALD-deposited AZO at GUNAM within Work Package 4 (Section 2.4). Another strategy for PCE improvement involves optimizing LiSo to identify the trade-off in process parameters that maximize V_{OC} improvement without increasing, or while reducing, R_S in SnO_X-based SHJ solar cells. Furthermore, upscaling SnO_X sputtering is planned which will enable the use of full wafers instead of

10 cm x 10 cm coupons. This, in turn, will help mitigate undesirable effects characteristic of small-area devices, such as V_{OC} reduction caused by perimeter recombination, which will consequently contribute to an increase in PCE.

2.4 sALD AZO

SiLEAN aims to achieve a completely indium-free transparent contact stack by eliminating the conventional ITO interlayer (Figure 1). To accomplish this, AZO deposited via sALD will be developed as a dedicated contact interlayer. The challenge is to fundamentally reduce the contact resistivity at the interface of the doped a-Si:H layers in these indium-free configurations. While SnO_x will be utilized as the bulk TCO due to its excellent optical transparency and lateral conductivity, its direct interface with doped a-Si:H can present electrical barriers. Therefore, a seed AZO:H layer will be incorporated directly between the SnO_x and the a-Si:H. In this combined stack, the AZO:H serves as a conductive buffer to improve charge carrier extraction, allowing the SnO_x overlayer to efficiently transport the current. The initial development and deposition parameters for these AZO layers were successfully established under Milestone 12 (**MS12**). The first target is to establish a baseline process with highly uniform and transparent layers over full wafer sizes. In a second stage, their electrical transport properties will be optimised. The details of this foundational first stage are given below.

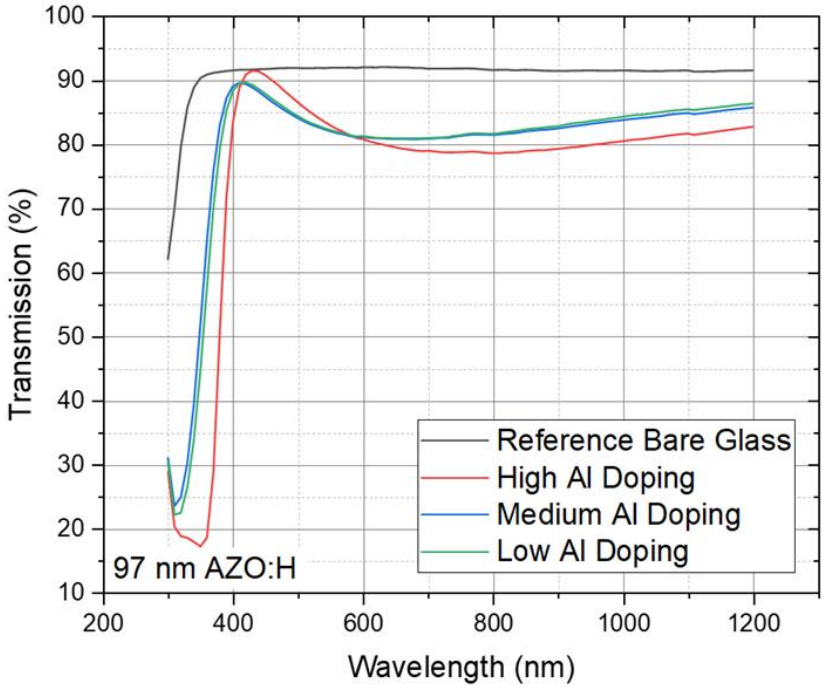

Figure 7: Transmission results for 97 nm AZO with varying Al doping ratios.

The transmission results for the initial Al doping flow study for AZO with around 97 nm are given in Figure 7. The high Al-doping sample exhibits characteristics of extreme overdoping, resulting in negligible conductivity (>MΩ/sq). Additionally, its transmission spectrum is significantly different than other AZO measurements with lower Al doping ratios and does not follow the general trend of Burstein-Moss shift in the literature [7][8], indicating structural alterations from standard AZO for this sample, possibly due to a highly increased ratio of Al_2O_3 clusters within the AZO matrix. Significantly lowering the DMAI flow by increasing the N_2 dilution flow from 2.5 slm to 9 (blue line in Figure 7) and 18 slm (green line in Figure 7), not only increases the transmission to >80% in the entire range of 380-1200 nm wavelength but also lowers the sheet resistance to 5.2 and 3.0 kΩ/sq,

respectively. Subsequently, the medium and low Al doping recipes were applied to thinner AZO layers (83.3 nm) to enhance transmission without compromising conductivity (Figure 8).

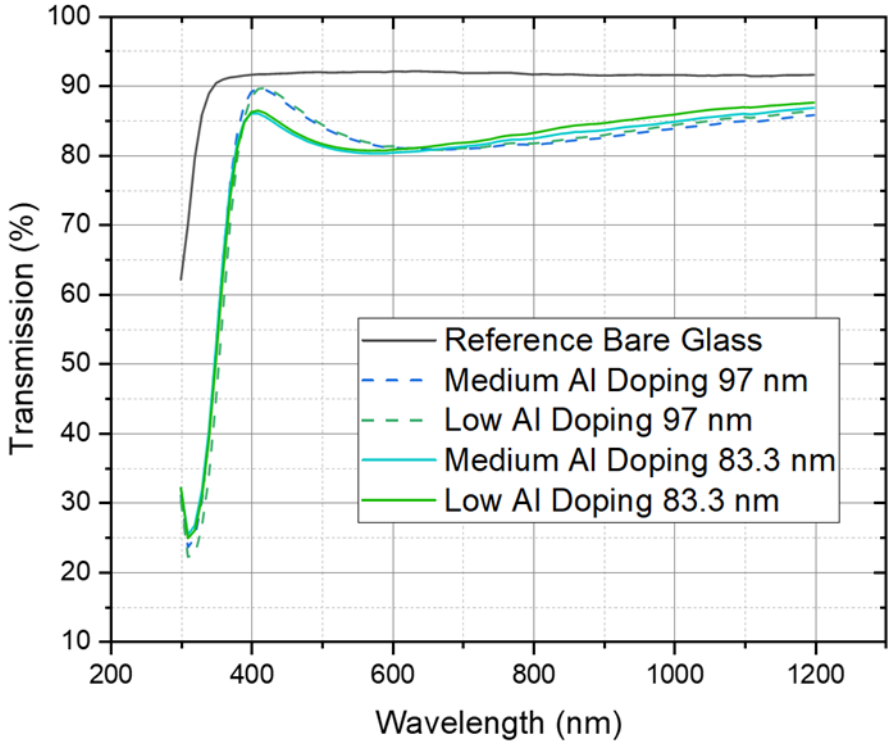

Figure 8: Transmission results for 83.3 nm and 97 nm AZO with varying Al doping ratios

This yielded slightly improved transmission at wavelengths above 600 nm while maintaining sheet resistance values similar to those of the 97 nm counterparts (5.8 and 3.5 kΩ/sq for medium and low doping samples (Table 2)).

Table 2: Sheet resistance values for AZO samples with different thicknesses and Al doping ratios.

	Sheet Resistance (kΩ/sq)		
AZO Thickness	*Low Al Doping*	*Medium Al Doping*	*High Al Doping*
83.3 nm	*3.5*	*5.8*	-
97 nm	*3.0*	*5.2*	*>1000*

Figure 9 represents the optical parameters of 83.3 nm AZO with an extinction coefficient (k) of 0.10 and a refractive index (n) of 1.77. Figure 9 shows a clear increase in k at low photon energies, which is common for TCOs and is an indicator of free carrier absorption within the layer [8]. The presence of this absorption tail confirms a high carrier density, which is consistent with the measured low sheet resistance values, as the same free electrons responsible for the optical absorption facilitate efficient charge transport.

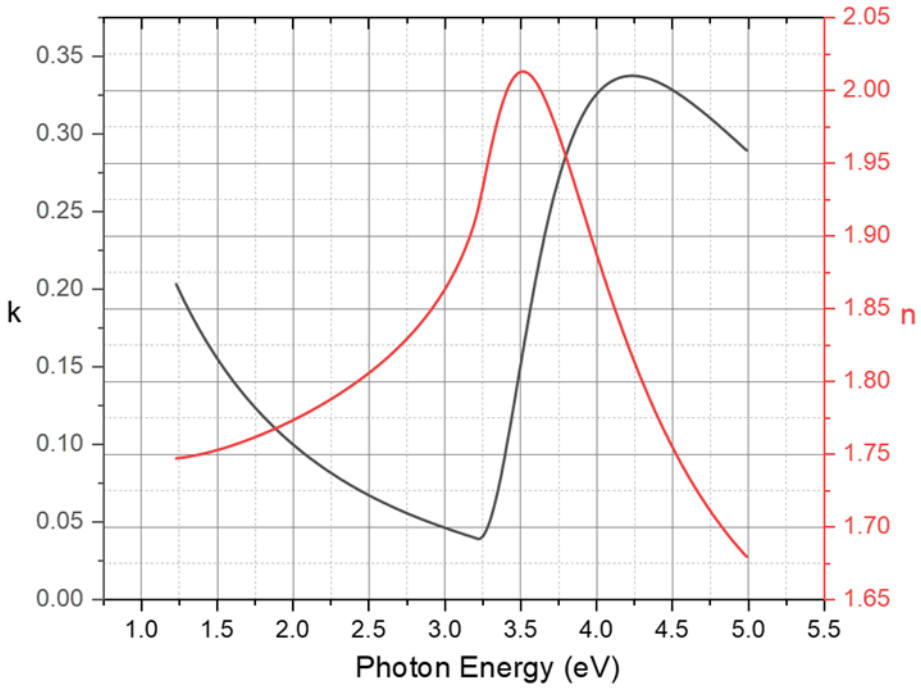

Figure 9: n-k measurements for 83.3 nm AZO

The experimental trend indicates that the fabricated AZO layers currently remain in the overdoped regime, as evidenced by the continuous increase in conductivity with reduced Al doping. However, further reducing the dopant concentration via the current co-injection method is restricted by hardware limitations. Specifically, lowering the DMAI flow below current levels induces mechanical instabilities, while increasing the N_2 dilution flow causes rapid temperature drops in the precursor tracing lines, thereby compromising the deposition conditions. To overcome these constraints, future optimization efforts will transition from co-injection to a supercycle deposition strategy. This approach will involve interleaving a few intrinsic ZnO layers between AZO layers, allowing for a precise reduction in the effective Al dopant concentration without triggering the instability issues associated with extremely low precursor flows.

2.5 Summary of the indium-free TCOs developed so far

The main optoelectrical properties of the TCOs developed so far in the project are summarized in Table 2, in comparison to ITO and AZO references.

Table 3: Optoelectrical properties of the best developed TCO so far for compared to reference sputtered ITO and sputtered AZO. The main pros and cons are also listed.

TCO	Resistivity (mOhm.cm)	Sheet resistance (Ohm/sq)	J_{loss} (mA/cm^2), d = 70 nm	Pros/Cons
Sputtered ITO	0.40	40	0.72	High conductance and transparency but In containing
Sputtered AZO	2.70	306	0.69	In-free but low ambient chemical stability (e.g

				moisture sensitivity)
PECVD ZnO	21.6	2057	0.35	In-free, high tunability but low throughput and poor ambient chemical stability
Sputtered SnO_X (0.6%, 100 W)	2.68	292	0.55	In-free, high ambient chemical stability but high contact resistivity at TCO/a-Si:H interface
Sputtered ITO (10 nm)/SnO_X (0.6%, 100 W)	2.04	199	0.93	High ambient chemical stability, low contact resistivity at TCO/a-Si:H interface but still contains In, although the In content is reduced by 80%
sALD AZO	Not available yet	3500	Not available yet	In-free and high layer conformality

The main photovoltaic parameters of the SHJ solar cells employing the developed SnO_X, ITO (10 nm)/SnO_X as contact layers are presented in Table 3, in comparison with the ITO reference.

Table 4: Electrical performance parameters of SHJ solar cells employing sputtered SnO_X and reference solar cells.

TCO type	In reduction rate	SHJ structure	V_{OC} [mV]	J_{SC} [mA/cm^2]	FF [%]	R_S [Ohm.cm^2]	PCE [%]
SnO_X (0.4%, 75W)	100%	FZJ	732	38.6	75.6	1.6	21.3
SnO_X (0.6%, 100 W)	100%	FZJ	732	38.5	76.6	1.5	21.6
SnO_X (1.0%, 150 W)	100%	FZJ	724	38.4	74.3	2.0	20.6
SnO_X (1.4%, 200 W)	100%	FZJ	695	37.7	69.8	2.6	18.3
Reference ITO	0%	FZJ	728	38.6	79.7	0.5	22.4
SnO_X (0.6%, 100 W)	100%	3SUN	733	38.6	74.0	2.2	20.9
ITO (10 nm)/SnO_X (0.6%, 100 W)	80%	3SUN	733	38.4	81.8	0.6	23.1
Reference ITO	0%	3SUN	731	38.7	81.7	0.6	23.1

2.6 Contribution to project (linked) Objectives

This deliverable contributes to the achievement of objective 3 demonstration of novel contacts for thin SHJ solar cells with a strong reduction of scarce materials, achieving sub-objective 3a (development of indium-free contact layers).

2.7 Contribution to major project exploitable result

This deliverable contributes to the building up of the exploitable results for the following processes and products: high-efficiency, high-reliability low-cost silicon solar cells.

3 Conclusion and Recommendations

As a result of the research, a PECVD-based approach for depositing undoped ZnO contact layers for SHJ solar cells was developed; however, the resulting films exhibited relatively high resistivity and poor stability under the air annealing. The introduction of sputtered GAZO, AZO, and ITO seed layers significantly improved the electrical properties and enabled successful integration into SHJ solar cells, increasing the PCE from 8.7% (undoped PECVD ZnO at the front side) to 19.4% (sputtered AZO/undoped PECVD ZnO/sputtered ITO at the front side). Nevertheless, further optimization of the PECVD process is required for further improvements in V_{OC} and FF. At present, the approach is constrained by a significant technical challenge, namely a sharp decrease in the deposition rate of undoped PECVD ZnO.

Sputtered SnO_X has been proposed as an indium-free alternative to undoped PECVD ZnO for SHJ solar cell contact layers. Systematic investigations allowed the optimization of the optoelectronic properties of the films, which were subsequently used as contact layers in fully indium-free (SnO_X only) and indium-lean (ITO seed layer/SnO_X) architectures.

The main limitation of SnO_X-based SHJ solar cells is the relatively high contact resistivity at SnO_X/a-Si:H interface, which reduces FF. A champion PCE of 22.0% was achieved for this indium-free architecture. Introducing a thin (10 nm) ITO seed layer significantly mitigates this issue, enabling champion PCE of 23.4% for ITO/SnO_X-based devices, which are comparable within the error margin to the 23.3.% achieved for reference ITO-based SHJ solar cells, while reducing the indium content by 80%.

Based on the results of this study, the following recommendations are proposed for further development and optimization:

1. **Further reduction of contact resistivity in indium-free configurations.** The following strategies will be employed: replacing doped a-Si:H with nc-Si(O_X):H layers, currently being developed at FZJ as part of an alternative transparent passivating contact within Work Package 3, and incorporating indium-free interlayers with improved contact properties, such as sputtered and/or sALD-grown AZO, between SnO_X and a-Si:H. The latter indium-free TCO is being developed at GUNAM.
2. **Optimizing LiSo process parameters** (temperature, time) to maximize V_{OC} without increasing – or even while simultaneously reducing - R_S.
3. **Upscaling SnO_X sputtering** to full M2/M2$^+$ wafer sizes which will avoid issues associated with small-area cells and potentially increase the PCE.

The innovations in contact layers introduced to date within the SiLEAN project together with the proposals for further improvements described above within the overall project framework, are illustrated in Figure 10.

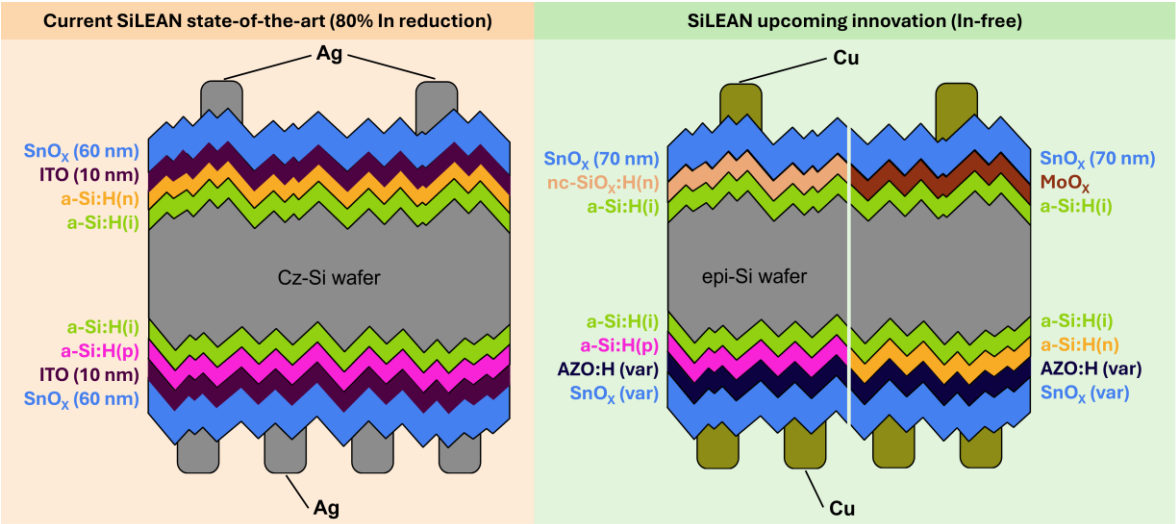

Figure 10: Current state-of-the-art in SiLEAN (left) and upcoming SiLEAN innovation (right) at SHJ solar-cell level.

4 Risks and interconnections

4.1 Risks/problems encountered

Risk No.	What is the risk	Probability of risk occurrence[1]	Effect of risk[1]	Solutions to overcome the risk
4	Upscaled SnO_X exhibit reduced conductivity - Section 2.1.2.	3	2	Further process development will be required. For sample exchange to Work Packages 3 and 5 and Task 4.4, we will then use AZO-based samples (including sALD-grown AZO) to keep the impact on other Work Packages as low as possible.

[1)] Probability risk will occur: 1 = high, 2 = medium, 3 = Low

4.2 Interconnections with other deliverables

The results described in this deliverable contribute to achieving D4.3 **> 25% solar cell with Ag-free contacts** and D5.3 **Record cell**.

5 Deviations from Annex 1

To circumvent the limitations associated with the low deposition rates of undoped PECVD ZnO and delays in upgrading the deposition chamber, FZJ has proposed replacing undoped PECVD ZnO with sputtered SnO_X. While SnO_X offers less flexibility in tuning the contact stack, it has already demonstrated superior optoelectrical performance compared to undoped PECVD ZnO, along with promising stability. Moreover, the initial results suggest reduced passivation damage in optimized regimes compared to sputtered ITO. In addition, sputtering provides significantly higher deposition rates, offering a clear advantage for upscaling. Although this transition may result in a delay of several months in upcoming deliverables, it is not expected to affect the overall project objectives.

6 References

1. Y. Wu, S.E. Potts, P.M. Hermkens, H.C.M. Knoops, F. Roozeboom, W.M.M. Kessels, Enhanced doping efficiency of al-doped ZnO by atomic layer deposition using dimethylaluminum isopropoxide as an alternative aluminum precursor, Chemistry of Materials 25 (2013) 4619–4622. https://doi.org/10.1021/CM402974J.
2. J. Pilz, A. Perrotta, P. Christian, M. Tazreiter, R. Resel, G. Leising, T. Griesser, and A. M. Coclite, "Tuning of material properties of ZnO thin films grown by plasma-enhanced atomic layer deposition at room temperature," *J. Vac. Sci. Technol. A*, vol. 36, no. 1, p. 01A109, 2018, doi: 10.1116/1.5003334.
3. M. D. Barankin, E. Gonzalez II, A. M. Ladwig, and R. F. Hicks, "Plasma-enhanced chemical vapor deposition of zinc oxide at atmospheric pressure and low temperature," *Solar Energy Materials and Solar Cells*, vol. 91, no. 10, pp. 924–930, 2007, doi: 10.1016/j.solmat.2007.02.009.
4. Cao Yu, Q. Zou, Q. Wang, Y. Zhao, X. Ran, G. Dong, C.-W. Peng, V. Allen, X. Cao, J. Zhou, Y. Zhao, and X. Zhang, "Silicon solar cell with undoped tin oxide transparent electrode," *Nature Energy*, vol. 8, no. 10, pp. 1119–1125, 2023, doi: 10.1038/s41560-023-01331-7.
5. T. Koida, T. Matsui, and H. Sai, "Amorphous SnO_2 as Earth-Abundant Stable Transparent Conductive Oxide and Its Application to Si Heterojunction Solar Cells," *Solar RRL*, vol. 7, no. 18, p. 2300381, 2023, doi: 10.1002/solr.202300381.
6. Q. Tang, W. Duan, A. Lambertz, K. Bittkau, M. A. Yaqin, Y. Zhao, K. Zhang, Q. Yang, D. Qiu, F. Gunkel, M. Weber, U. Rau, and K. Ding, ">85% indium reduction for high-efficiency silicon heterojunction solar cells with aluminum-doped zinc oxide contacts," *Solar Energy Materials and Solar Cells*, vol. 249, p. 111748, 2023, doi: 10.1016/j.solmat.2022.112120.
7. H.C.M. Knoops, B.W.H. van de Loo, S. Smit, M. V. Ponomarev, J.-W. Weber, K. Sharma, W.M.M. Kessels, M. Creatore, Optical modeling of plasma-deposited ZnO films: Electron scattering at different length scales, Journal of Vacuum Science & Technology A 33 (2015). https://doi.org/10.1116/1.4905086.
8. B. Macco, B.W.H. van de Loo, M. Dielen, D.G.J.A. Loeffen, B.B. van Pelt, N. Phung, J. Melskens, M.A. Verheijen, W.M.M. Kessels, Atomic-layer-deposited Al-doped zinc oxide as a passivating conductive contacting layer for n+-doped surfaces in silicon solar cells, Solar Energy Materials and Solar Cells 233 (2021) 111386. https://doi.org/10.1016/J.SOLMAT.2021.111386.

7 Acknowledgement

The author(s) would like to thank the partners in the project for their valuable comments on previous drafts and for performing the review.

Project partners:

#	Partner short name	Partner Full Name
1	FZJ	FORSCHUNGSZENTRUM JULICH GMBH
2	IMEC	INTERUNIVERSITAIR MICRO-ELECTRONICA CENTRUM
3	TUD	TECHNISCHE UNIVERSITEIT DELFT
4	UNR	UNIRESEARCH BV
5	NXW	NEXWAFE GMBH
6	PVW	PV Works B.V.
7	GET	GraphEnergyTech
8	3SUN	3SUN S.R.L.
9	GUNAM	ODTU GUNES ENERJISI UYGULAMA VE ARASTIRMA MERKEZI

This project has received funding from the European Union's Horizon Europe research and innovation programme under grant agreement No 101147275. Views and opinions expressed are however those of the author(s) only and do not necessarily reflect those of the European Union. Neither the European Union nor the granting authority can be held responsible for them.

8 Appendix A - Quality Assurance Review Form

The following questions should be answered by all reviewers (WP Leader, reviewer, Project Coordinator) as part of the Quality Assurance procedure. Questions answered with NO should be motivated. The deliverable author will update the draft based on the comments. When all reviewers have answered all questions with YES, only then can the Deliverable be submitted to the EC. NOTE: This Quality Assurance form will be removed from Deliverables with dissemination level "Public" before publication.

Question	**WP Leader**	**Reviewer**	**Project Coordinator**
	Valerie Depauw (IMEC)	Olindo Isabella (TUD)	Karsten Bittkau (FZJ)
1. *Do you accept this Deliverable as it is?*	Yes	Yes	Yes
2. *Is the Deliverable complete?* - *All required chapters?* - *Use of relevant templates?*	Yes	Yes	Yes
3. *Does the Deliverable correspond to the DoA?* - *All relevant actions performed and reported?*	Yes	Yes	Yes
4. *Is the Deliverable in line with the SiLEAN objectives?* - *WP objectives* - *Task Objectives*	Yes	Yes	Yes
5. *Is the technical quality sufficient?* - *Inputs and assumptions correct/clear?* - *Data, calculations, and motivations correct/clear?* - *Outputs and conclusions correct/clear?*	Yes	Yes	Yes
6. *Is created and potential IP identified and are protection measures in place?*	N.A.	N.A.	N.A.
7. *Is the Risk Procedure followed and reported?*	Yes	Yes	Yes
8. *Is the reporting quality sufficient?* - *Clear language* - *Clear argumentation* - *Consistency* - *Structure*	Yes	Yes	Yes